

Stability and strength of monolayer polymeric C₆₀

Bo Peng^{1,*}

¹*Theory of Condensed Matter Group, Cavendish Laboratory, University of Cambridge,
J. J. Thomson Avenue, Cambridge CB3 0HE, United Kingdom*

(Dated: January 6, 2023)

Two-dimensional fullerene networks have been synthesized in several forms [Hou *et al.*, *Nature* **2022**, 606, 507], and it is unknown which monolayer form is stable at ambient condition. Using first principles calculations, I show that the believed stability of the quasi-tetragonal phases is challenged by mechanical, dynamic or thermodynamic stability. For all temperatures, the quasi-hexagonal phase is thermodynamically least stable. However, the relatively high dynamic and mechanical stabilities suggest that the quasi-hexagonal phase is intrinsically stronger than the other phases under various strains. The origin of the high stability and strength of the quasi-hexagonal phase can be attributed to the strong covalent C–C bonds that strongly hold the linked C₆₀ clusters together, enabling the closely packed hexagonal network. These results rationalize the experimental observations that so far only the quasi-hexagonal phase has been exfoliated experimentally as monolayers.

Recent attempts to synthesize layers of connected buckyballs, i.e. C₆₀ molecules linked by carbon–carbon bonds, have obtained different arrangements of cluster cages through the formation of bonds between neighboring C₆₀ molecules [1]. The obtained allotropes include a few-layer rectangular structure in which each C₆₀ molecule has four neighboring buckyballs and a monolayer hexagonal structure in which each C₆₀ cage binds to six neighbors, namely, a few-layer quasi-tetragonal phase (qTP) and a monolayer quasi-hexagonal phase (qHP) respectively. Great efforts have been devoted to stabilizing the linking bonds between neighboring cluster cages by introducing magnesium atoms to form a quasi-2D fullerene network with strong intralayer covalent bonds [1] because Mg atoms tend to promote covalent bonds [2, 3]. To aid exfoliation, the Mg ions that hold the C₆₀ cages together can be then replaced by large organic ions, which can be removed afterwards by hydrogen peroxide, leading to pure, charge neutral fullerene networks in 2D [1, 4]. Unfortunately, only qHP C₆₀ has been obtained as monolayers, while all the qTP C₆₀ flakes are few-layer [1]. These results raise doubts regarding the stability of monolayer fullerene networks.

Ever since the discovery of C₆₀ [5], the formation mechanism and stability of the fullerene molecules are far from completely understood [6–9]. When forming structural units of C₆₀ clusters in a 2D plane, it is unclear whether ordered structures of monolayer polymeric C₆₀ are stable under ambient conditions such as strain and temperature. Recent first principles calculations have investigated various structural phases of monolayer C₆₀ with different bonding characters [10–15]. The mechanical stability of several phases has been confirmed [10, 11, 14]. More recently, the thermal stability of monolayer C₆₀ has been addressed using molecular dynamics simulations, showing that both qTP and qHP C₆₀ monolayers can remain stable at temperatures near 800 K [16], which is partially consistent with the experimental result that monolayer

qHP C₆₀ does not decompose at 600 K [1]. However, previous analysis based on mechanical and thermal stability cannot explain why the qTP monolayers have not yet been exfoliated experimentally. Furthermore, the dynamic stability of monolayer fullerene networks with respect to lattice vibrations, which indicates whether the crystal structure is in a local minimum of the potential energy surface [17–20], is still unexplored. Additionally, the thermodynamic stability of different phases, which energetically classifies the stability (especially at finite temperatures) [21–33], remains unknown. Because of such knowledge gaps, several questions need to be answered to understand the phase stability of monolayer fullerene networks: (i) Are qTP and qHP C₆₀, as pure carbon monolayers without extra Mg or organic ions to bind the C₆₀ cages together, dynamically stable? (ii) What is their relative stability in a thermodynamic aspect? (iii) Can the calculated mechanical strength support their phase stability?

In this work, I investigate the mechanical, dynamic and thermodynamic stability of monolayer qTP and qHP C₆₀ by using first principles calculations. Structural relaxation obtains two crystal structures of the quasi-tetragonal phase (denoted as qTP1 and qTP2 respectively). I show that the qTP1 monolayer, albeit being thermodynamically stable at all temperatures above 380 K, possesses low dynamic and mechanical stability due to its weak bonding perpendicular to the straight chains of C₆₀ buckyballs. On the other hand, although qTP2 fullerene might be the ground-state structure with the lowest Gibbs free energy at 0 K and exhibits good dynamic and mechanical stability, it is only thermodynamically stable with respect to qTP1 C₆₀ at low temperatures. Instead, monolayer qHP C₆₀ should be experimentally accessible owing to their dynamic and mechanical stability, in spite of its lowest thermodynamic stability among all three phases. In addition, qHP C₆₀ has the highest strength under various strains (hydrostatic, uni-

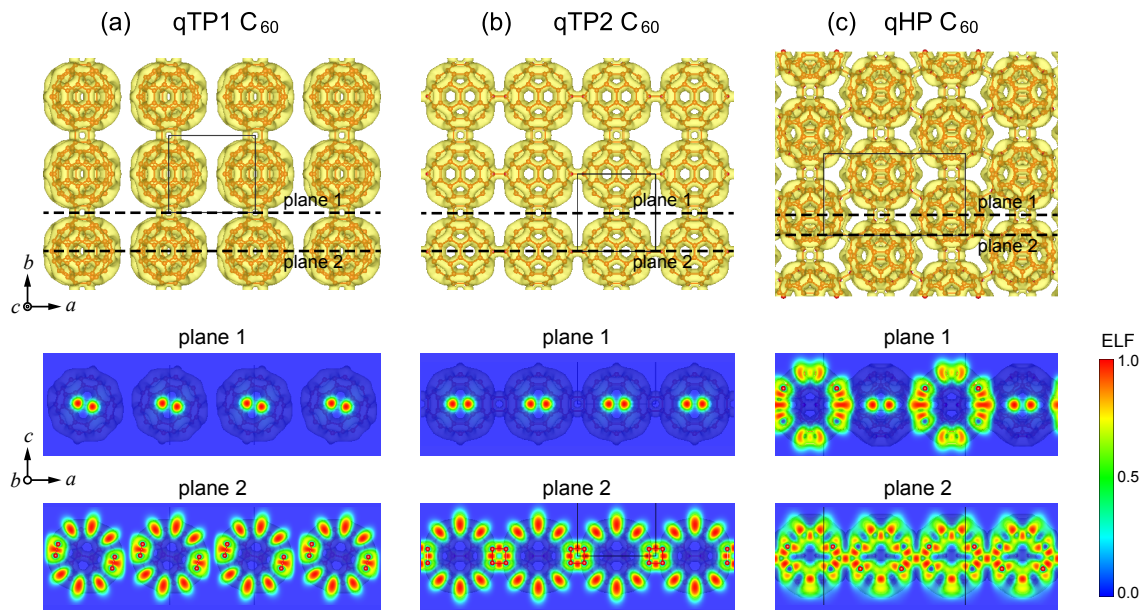


FIG. 1. Bond structures for (a) qTP1, (b) qTP2 and (c) qHP C_{60} . The default isosurface level in VESTA [39] is used. Maps of the ELF on the (010) plane are also present.

axial and shear) because of the closely packed crystal structures.

First principles calculations are performed using the Vienna *ab-initio* simulation package (VASP) [34, 35]. The projector augmented wave (PAW) potential is used with C $2s^2 2p^2$ valence states [36, 37], under the generalized gradient approximation (GGA) with the Perdew-Burke-Ernzerhof parameterization revised for solids (PBEsol) as the exchange-correlation functional [38]. The crystal structures are optimized by fully relaxing the lattice constants and internal atomic coordination (for computational details, see the Supporting Information). Geometry optimization starting from the quasi-tetragonal phase consisting of only carbon atoms leads to a quasi-1D qTP monolayer (qTP1), as shown in Fig. 1(a). On the other hand, a two-step structural relaxation, starting from monolayer qTP Mg_2C_{60} and then removing the Mg ions before the second relaxation, obtains a tightly bound qTP monolayer (qTP2), as shown in Fig. 1(b). The two-step structure relaxation mimics the experimental procedure to remove the charged ions introduced during synthesis [1, 4]. The computed lattice constants for all three phases are listed in Table I, which are in good agreement with previous results [10, 11, 15], therefore confirming the reliability of the present calculations.

The bond structures at equilibrium are examined in Fig. 1. The relaxed structure for qTP1 fullerene can be regarded as one-dimensional chains of C_{60} cages along the b direction that are linked by the nearly in-plane [2+2] cycloaddition bonds. In comparison, qTP2 fullerene is a two-dimensional network of C_{60} cages connected by the

TABLE I. Calculated static lattice constants (in Å) and cohesive energy E_c (in eV/atom) of qTP1, qTP2 and qHP C_{60} monolayers, 1D qTP C_{60} chain and 0D C_{60} molecule. The cohesive energy is defined as $E_c = E_{tot}/N - E_{isolated}$, where E_{tot} is the total energy of the crystal, N is the number of atoms in the unit cell and $E_{isolated}$ is the total energy of an isolated carbon atom. The room-temperature lattice constants calculated under the quasi-harmonic approximation are also listed in parentheses for comparison.

phase	a	b	E_c
2D qTP1	10.491 (10.522)	9.063 (9.090)	-9.2582
2D qTP2	9.097 (9.132)	9.001 (9.031)	-9.2587
2D qHP	15.848 (15.896)	9.131 (9.162)	-9.2465
1D	9.062 (9.098)	-	-9.2579
0D	-	-	-9.2564

out-of-plane vertical [2+2] cycloaddition bonds along the a direction and the in-plane [2+2] cycloaddition bonds along the b direction. The major difference between qTP1 and qTP2 is the absence of the vertical [2+2] cycloaddition bonds along a in the former. Regarding the qHP monolayer, the C_{60} cages form a hexagonal network through the similar planar [2+2] cycloaddition bonds along the b direction and C-C single bonds along the

TABLE II. Elastic properties for qTP1, qTP2 and qHP C_{60} , with the elastic constants C_{ij} , shear modulus G^{2D} , layer modulus γ , Young's modulus Y^{2D} in N/m, and Poisson's ratio ν dimensionless. The elastic constants C_{11} , C_{22} and C_{66} calculated from phonon speed of sound are also listed in parentheses for comparison.

phase	C_{11}	C_{22}	C_{12}	$C_{66} = G^{2D}$	γ	Y_a^{2D}	Y_b^{2D}	ν_a	ν_b
qTP1	5.4 (2.5)	123.7 (121.3)	-1.2 -	-0.2 -	31.7	5.4	123.5	-0.010	-0.225
qTP2	149.9 (150.5)	148.7 (141.2)	22.9 -	53.4 (54.5)	86.1	146.4	145.2	0.154	0.153
qHP	150.8 (142.4)	186.8 (172.7)	22.5 -	60.6 (61.7)	95.6	148.1	183.4	0.120	0.149

other two directions diagonal to the rectangular unit cell.

Figure 1 also shows the maps of the electron localization function (ELF) on the (010) plane. A high value of ELF indicates strong electron localization [40–43]. As shown in Fig. 1(a), the covalent [2+2] bonds along b in qTP1 fullerene lead to high electron localization there (plane 1), whereas no bonds are formed between neighboring C_{60} cages along a (plane 2). In contrast, the vertical [2+2] bonds along a in qTP2 fullerene result in high electron localization between neighboring C_{60} cages, as demonstrated in plane 2 of Fig. 1(b). For qHP C_{60} , the hexagonal network has higher electron localization in both directions, as one can see from Fig. 1(c). As a result, one can expect that the hexagonal networks should stabilize and strengthen the structure of qHP C_{60} , making it slightly more stable than qTP2 C_{60} while much more stable than qTP1 C_{60} . However, as shown below, although the mechanical and dynamic stabilities are consistent with the ELF picture, high electron localization in qHP C_{60} does not guarantee their thermodynamic stability.

To confirm the mechanical stability, the elastic constants are calculated by finite differences through finite distortions of the lattice [44, 45]. There are different ways to define the 2D elastic constants from the computed 3D coefficients [17, 46, 47]. Here the 2D coefficients C_{ij}^{2D} are renormalized by the c lattice constant (the spacing between 2D layers) [17, 46], i.e. $C_{ij}^{2D} = c \times C_{ij}^{3D}$. The obtained 2D elastic constants (including ionic relaxations) are listed in Table II using the Voigt notation: $1 - xx$, $2 - yy$, $6 - xy$, and the present results agree well with previous calculations [10, 11]. According to Born-Huang's lattice dynamical theory [48, 49], in monoclinic crystals (qTP1 and qHP with space group $P2/m$ and Pc respectively), the mechanical stability criteria is given by

$$C_{11} > 0, C_{22} > 0, C_{66} > 0, C_{11} + C_{22} + 2C_{12} > 0. \quad (1)$$

In orthorhombic crystals (qTP2 C_{60} with space group $Pmmm$), the Born stability criteria has an extra require-

ment in addition to Eq. (1)

$$C_{11} + C_{22} - 2C_{12} > 0. \quad (2)$$

The elastic constants of qTP2 and qHP C_{60} satisfy their corresponding criteria, indicating that they are mechanically stable. Interestingly, the shear strength G^{2D} of qTP1 C_{60} is negative, demonstrating its low shear resistance. The 1D chains in qTP1 C_{60} are prone to bending under shear deformation, which may lead to a sliding of C_{60} chains and even lattice instability. In addition, C_{11} in qTP1 fullerene is more than one order of magnitude lower than C_{22} . Such weak stiffness is correlated to weak interchain bonding effect along a as discussed above and the weak dynamic stability as will be demonstrated below. In contrast, C_{11} and C_{22} are nearly the same in qTP2 fullerene because of the similar [2+2] cycloaddition bonds along both a and b . For qHP fullerene, the elastic constants C_{11} , C_{22} and C_{66} are the highest among the three phases, in consistent with the high electron localization in the hexagonal networks that strengthens the crystal structure.

The strength of monolayer fullerene networks is obtained from the computed elastic constants, as summarized in Table II. The layer modulus γ is the 2D equivalent to the bulk modulus, which measures the resistance to hydrostatic stretching in 2D materials [50]. The layer moduli show an increasing trend from qTP1 to qTP2 and to qHP C_{60} . The γ for qTP2 C_{60} is more than twice that of qTP1 C_{60} , while slightly lower than that of qHP C_{60} , which concurs with the bonding structures of three fullerene networks. In general, qTP2 and qHP C_{60} have comparable moduli and therefore similar hardness properties, whereas qTP1 C_{60} has less resilience to both shear and hydrostatic strains.

The anisotropy of strength is also investigated by calculating the Young's modulus and Poisson's ratio. In qTP1 fullerene, the Young's modulus Y^{2D} along a is more than 22 times lower than that along b , indicating that qTP1 C_{60} is much less structurally rigid to elongations along a . In qTP2 C_{60} , the Young's moduli along a

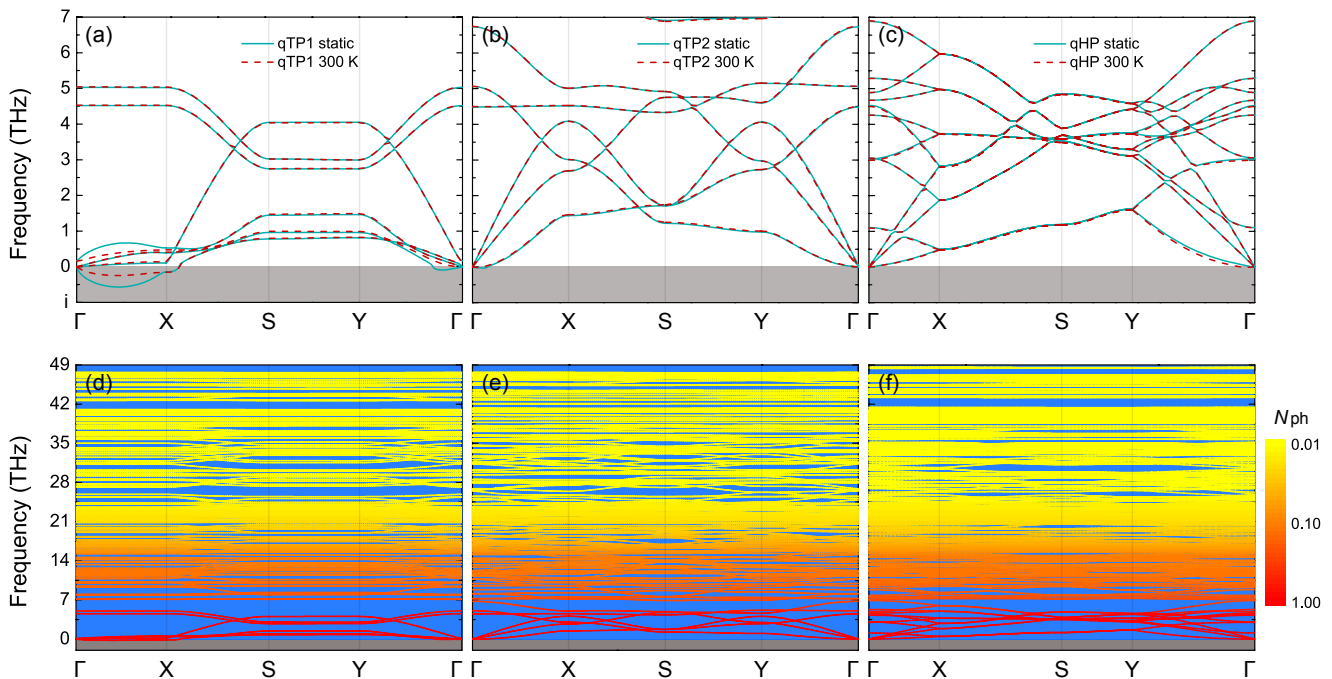


FIG. 2. Low-frequency phonons of (a) qTP1, (b) qTP2 and (c) qHP C_{60} using the static and room-temperature lattice constants. Entire phonon spectra for (d) qTP1, (e) qTP2 and (f) qHP C_{60} using the room-temperature lattice constants, with the phonon occupation number N_{ph} determined from the Bose-Einstein distribution function at 300 K.

and b are nearly the same due to similar $[2+2]$ cycloaddition bonds along both directions, showing that they have the same resilience to linear strain. Regarding the qHP monolayers, the Y_a^{2D} has a value 80% the Y_b^{2D} , indicating slightly weaker stiffness of the C–C single bonds in the presence of strain along a . The Poisson's ratio ν for qTP1 C_{60} is negative, i.e. the qTP1 fullerene monolayers expand laterally when stretched, and the $|\nu_a|$ is significantly lower than $|\nu_b|$ because of much less bond stretching under uniaxial strain. Monolayer qTP2 C_{60} has a nearly isotropic ν of $0.153 - 0.154$, while the ν_a in qHP fullerene is slightly lower than ν_b . These results indicate that qTP1 C_{60} is unable to withstand greater strains along a than those along b , which is the origin of its overall low strength.

To evaluate the dynamic stability of monolayer fullerene networks, lattice dynamical properties are calculated within the harmonic approximation based on density functional perturbation theory [51–53]. The phonon spectra of all three phases are gathered in Fig. 2. As shown in Fig. 2(a), the phonon dispersion of qTP1 C_{60} using the static lattice constants exhibits small imaginary frequency ($< 0.6i$ THz) along the entire Γ -X high-symmetry line. An imaginary frequency indicates a decrease in potential energy when the atoms are displaced away from their equilibrium positions, corresponding to a non-restorative force [20]. Therefore, the imaginary frequency along Γ -X implies that monolayer qTP1 C_{60}

can be split into individual 1D chains in the presence of interchain (out-of-plane) vibrations, demonstrating its weak dynamic stability along the a direction. There is a fourth mode at Γ with nearly zero frequency in qTP1 C_{60} , which, sometimes known as the torsional acoustic mode, is a strong indication of the (quasi-)1D nature [54, 55]. The thermal expansion is included by computing the Gibbs free energy under the quasi-harmonic approximation [56–58], and the room-temperature lattice constants are listed in Table I. At 300 K, the imaginary mode in qTP1 C_{60} remains along Γ -X, though the imaginary frequency becomes smaller ($< 0.2i$ THz). In contrast, qTP2 and qHP fullerene are dynamically more stable as there is no imaginary mode in Fig. 2(b) and (c) using both the static and room-temperature lattice constants, indicating these structures are a local minimum on the potential energy surface and the atoms vibrate harmonically around their equilibrium positions.

From the phonon speed of sound, the elastic constants C_{11} , C_{22} and C_{66} can be calculated [59] (for details on the phonon group velocity, see the Supporting Information). As shown in Table II, the calculated elastic constants are in reasonably good agreement with those computed from the finite difference method [44, 45]. Moreover, qHP fullerene has the highest speed of sound along b and the highest phonon frequency with four phonon branches higher than 48.4 THz throughout the entire Brillouin zone, whereas the highest phonon frequencies

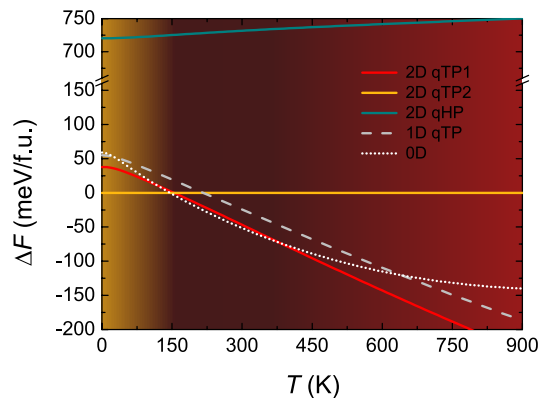


FIG. 3. Relative thermodynamic stability of monolayer fullerene networks, one-dimensional fullerene chain and zero-dimensional fullerene molecule, with the Gibbs free energy F of monolayer qTP2 C_{60} set to zero to compare the relative stability.

in qTP1 and qTP2 fullerene are lower than 47.7 THz, which is in line with the high mechanical strength in qHP C_{60} .

To clarify the thermodynamic stability of C_{60} monolayers, the cohesive energy is calculated, as listed in Table I. The resulting E_c of qTP2 fullerene is 0.5 meV/atom (30 meV per formula unit) lower than qTP1 and 12.2 meV/atom (732 meV per formula unit) lower than qHP, suggesting its thermodynamic stability. However, because the energy difference between the qTP1 and qTP2 monolayers is quite small, phonons can play an important role in determining the thermodynamic stability at both 0 K and finite temperatures [21–24]. The contribution of phonons can be examined by calculating the Gibbs free energy F [60–62]

$$F = \min_{a,b} \left[E_{\text{tot}} + \frac{1}{2} \sum_{\lambda} \hbar \omega_{\lambda} + k_B T \sum_{\lambda} \ln(1 - e^{-\hbar \omega_{\lambda} / k_B T}) \right], \quad (3)$$

where $\min_{a,b}[\]$ finds unique minimum value in the brackets by changing the lattice constants a and b to include thermal expansion, E_{tot} is the total energy of the crystal, \hbar is the reduced Planck constant, ω_{λ} is the phonon frequency at mode λ , k_B is the Boltzmann constant, and T is the temperature. The second term in Eq. (3) is temperature-independent, corresponding to the zero point energy (ZPE) of phonons; and the last term refers to the thermally excited population of phonons, as demonstrated by the Bose-Einstein distribution N_{ph} at 300 K in Fig. 2(d)-(f).

To quantify the relative thermodynamic stability at finite temperatures, the difference in Gibbs free energy ΔF with respect to the free energy of monolayer qTP2 C_{60} is plotted as a function of temperature T for all three phases, as illustrated in Fig. 3. With increasing

temperature, the free energy of qTP1 C_{60} drops faster than that of qTP2 C_{60} owing to their smaller vibrational frequencies. According to Eq. (3), smaller vibrational frequencies give rise to lower free energy and higher entropy (for details on the phonon density of states and entropy, see the Supporting Information), which is similar to the case in α - and β -tin [21, 22]. At 150 K, monolayer qTP1 C_{60} becomes thermodynamically more stable than the other two phases. At 300 K, the free energy of qTP1 C_{60} lies 47 meV per formula unit (meV/f.u.) below that of qTP2 C_{60} . At higher temperatures, the difference becomes even larger, further stabilizing the qTP1 structure in a thermodynamic perspective.

To further explore the thermodynamic stability of C_{60} in different dimensions, the monolayer qTP1 network is further isolated into 1D qTP C_{60} chain and 0D C_{60} molecule (for details about 1D and 3D C_{60} , see the Supporting Information). The cohesive energy E_c of 1D qTP C_{60} and 0D C_{60} is listed in Table I. Interestingly, the E_c of 1D qTP C_{60} chain is higher than monolayer qTP1 and qTP2 C_{60} network by merely 0.3 and 0.8 meV/atom respectively (18 and 48 meV/f.u.), whereas 11.4 meV/atom (684 meV/f.u.) lower than the E_c of 2D qHP C_{60} . The difference in E_c between 1D qTP C_{60} chain and monolayer qTP1 C_{60} network is even lower than the thermal fluctuation energy $k_B T$ at room temperature (26 meV), implying that 2D qTP1 C_{60} can be transformed into 1D chains in the presence of thermal fluctuations. Taking the finite temperature effects into account, the Gibbs free energy of 1D qTP C_{60} chain and the Helmholtz free energy of 0D C_{60} molecule are shown in Fig. 3 as a function of temperature. The Gibbs free energy of 1D qTP C_{60} chain is higher than that of 2D qTP1 C_{60} in the entire temperature range (0–900 K), and their free energy difference is 22 meV/f.u. at 300 K. On the other hand, the free energy of 1D qTP C_{60} chain becomes lower than that of 2D qTP2 C_{60} at temperatures above 220 K. Most interestingly, the free energy of 0D C_{60} molecule drops faster than all the other phases below room temperature, and becomes lower than 2D qTP1 and qTP2 C_{60} at 120 and 150 K respectively. However, the free energy of 2D qTP1 C_{60} decreases the fastest above room temperature, and consequently 2D qTP1 C_{60} is energetically more favored than all the other phases at temperatures above 380 K. As a result, monolayer qTP2 C_{60} is thermodynamically most stable at temperatures below 150 K, 0D C_{60} molecule has the lowest energy for temperatures between 150 and 380 K, and 2D qTP1 C_{60} is thermodynamically favored above 380 K.

Looking back at the calculated mechanical properties and stabilities, they seem in line with the experimental findings. It has been reported that fullerene monolayers can only be isolated experimentally for the honeycomb structure qHP, whereas the obtained rectangular structure qTP is few-layered [1]. Although qTP2 C_{60} is thermodynamically favored over qTP1 C_{60} at low tempera-

tures, clearly qTP1 C₆₀ is thermodynamically more stable than the other two phases at all temperatures above 150 K. However, thermodynamic stability of qTP1 C₆₀ does not guarantee high dynamic stability in the presence of interchain (out-of-plane) vibrations perpendicular to the quasi-1D chains. In addition, the low moduli and strength of qTP1 C₆₀ originated from the chain crystal structures, in addition to its low shear resistance, indicate that qTP1 C₆₀ cannot be intrinsically resilient under deformation. Moreover, monolayer qTP1 C₆₀ is thermodynamically less stable than 0D C₆₀ molecule for temperatures between 120 and 380 K. These results indicate the plausibility that monolayer qTP1 fullerene network can be further split into individual 1D chains or 0D molecules by thermal fluctuations, interchain acoustic vibrations, or external strains. In contrast, qHP C₆₀ is both dynamically and mechanically more stable with respect to qTP1 C₆₀. Therefore, monolayer polymeric C₆₀ has so far only been exfoliated from the quasi-hexagonal bulk single crystals. These results indicate that a systematic analysis of mechanical, dynamic and thermodynamic stabilities is necessary to rationalize the experimental data.

In conclusion, I carry out first principles calculations to evaluate the mechanical, dynamic and thermodynamic stabilities of qTP1, qTP2 and qHP C₆₀ monolayers, which have been so far believed to be stable. Electron localization analysis reveals that the low mechanical and dynamic stabilities in qTP1 fullerene are associated with the lack of C–C bonds connecting the adjacent C₆₀ chains, which also limits its achievable strength. Monolayer qTP2 C₆₀ is thermodynamically more stable at temperatures below 150 K, while thermally populated phonons hinder its thermodynamic stability with increasing temperature. The relatively high moduli of qHP fullerene indicate that it has a high strength because of the closely packed hexagonal fullerene network linked through both [2+2] cycloaddition bonds and C–C single bonds. This, in combination with the phonon stability, endows monolayer qHP C₆₀ with high stability and strength.

ACKNOWLEDGEMENTS

I thank Prof. Bartomeu Monserrat and Dr. Ivona Bravić at the University of Cambridge for helpful discussions. I acknowledge support from the Winton Programme for the Physics of Sustainability, and from Magdalene College Cambridge for a Nevile Research Fellowship. The calculations were performed using resources provided by the Cambridge Tier-2 system, operated by the University of Cambridge Research Computing Service (www.hpc.cam.ac.uk) and funded by EPSRC Tier-2 capital grant EP/P020259/1, as well as with computational support from the U.K. Materials and Molecular Modelling Hub, which is partially funded by EP-

SRC (EP/P020194), for which access is obtained via the UKCP consortium and funded by EPSRC grant ref. EP/P022561/1.

-
- * bp432@cam.ac.uk
- [1] Hou, L.; Cui, X.; Guan, B.; Wang, S.; Li, R.; Liu, Y.; Zhu, D.; Zheng, J. Synthesis of a monolayer fullerene network. *Nature* **2022**, *606*, 507–510.
 - [2] Pontiroli, D.; Aramini, M.; Gaboardi, M.; Mazzani, M.; Gorreri, A.; Riccò, M.; Margiolaki, I.; Sheptyakov, D. Ionic conductivity in the Mg intercalated fullerene polymer Mg₂C₆₀. *Carbon* **2013**, *51*, 143–147.
 - [3] Tanaka, M.; Yamanaka, S. Vapor-Phase Growth and Structural Characterization of Single Crystals of Magnesium Doped Two-Dimensional Fullerene Polymer Mg₂C₆₀. *Crystal Growth & Design* **2018**, *18*, 3877–3882.
 - [4] Gottfried, J. M. Molecular soccer balls connected to make a 2D material. *Nature* **2022**, *606*, 470–471.
 - [5] Kroto, H. W.; Heath, J. R.; O’Brien, S. C.; Curl, R. F.; Smalley, R. E. C₆₀: Buckminsterfullerene. *Nature* **1985**, *318*, 162–163.
 - [6] Kroto, H. W. The stability of the fullerenes C_n, with n = 24, 28, 32, 36, 50, 60 and 70. *Nature* **1987**, *329*, 529–531.
 - [7] Kroto, H. C₆₀, fullerenes, giant fullerenes and soot. *Pure and Applied Chemistry* **1990**, *62*, 407–415.
 - [8] Goroff, N. S. Mechanism of Fullerene Formation. *Acc. Chem. Res.* **1996**, *29*, 77–83.
 - [9] Bernal, J. J.; Haenecour, P.; Howe, J.; Zega, T. J.; Amari, S.; Ziurys, L. M. Formation of Interstellar C₆₀ from Silicon Carbide Circumstellar Grains. *The Astrophysical Journal Letters* **2019**, *883*, L43.
 - [10] Tromer, R. M.; Ribeiro, L. A.; Galvão, D. S. A DFT study of the electronic, optical, and mechanical properties of a recently synthesized monolayer fullerene network. *Chemical Physics Letters* **2022**, *804*, 139925.
 - [11] Yu, L.; Xu, J.; Peng, B.; Qin, G.; Su, G. Anisotropic Optical, Mechanical, and Thermoelectric Properties of Two-Dimensional Fullerene Networks. *J. Phys. Chem. Lett.* **2022**, *13*, 11622–11629.
 - [12] Yuan, D.; Pi, H.; Jiang, Y.; Zhou, Y. H. L.; Jia, Y.; Su, G.; Fang, Z.; Weng, H.; Ren, X.; Zhang, W. Highly in-plane anisotropic optical properties of fullerene monolayers. *arXiv:2207.11366* **2022**,
 - [13] Peng, B. Monolayer Fullerene Networks as Photocatalysts for Overall Water Splitting. *J. Am. Chem. Soc.* **2022**, *144*, 19921–19931.
 - [14] Ying, P.; Dong, H.; Liang, T.; Fan, Z.; Zhong, Z.; Zhang, J. Atomistic insights into the mechanical anisotropy and fragility of monolayer fullerene networks using quantum mechanical calculations and machine-learning molecular dynamics simulations. *Extreme Mechanics Letters* **2023**, *58*, 101929.
 - [15] Dong, H.; Cao, C.; Ying, P.; Fan, Z.; Qian, P.; Su, Y. Anisotropic and high thermal conductivity in monolayer quasi-hexagonal fullerene: A comparative study against bulk phase fullerene. *arXiv:2208.03982* **2022**,
 - [16] Ribeiro, L.; Pereira, M.; Giozza, W.; Tromer, R.; Galvão, D. S. Thermal stability and fracture patterns of a recently synthesized monolayer fullerene network: A reactive molecular dynamics study. *Chemical Physics*

- Letters **2022**, *807*, 140075.
- [17] Peng, B.; Zhang, H.; Shao, H.; Ning, Z.; Xu, Y.; Ni, G.; Lu, H.; Zhang, D. W.; Zhu, H. Stability and strength of atomically thin borophene from first principles calculations. *Materials Research Letters* **2017**, *5*, 399–407.
- [18] Malyi, O. I.; Sopiha, K. V.; Persson, C. Energy, Phonon, and Dynamic Stability Criteria of Two-Dimensional Materials. *ACS Appl. Mater. Interfaces* **2019**, *11*, 24876–24884.
- [19] Luo, D.; Yin, K.; Dronskowski, R. Existence of BeCN₂ and Its First-Principles Phase Diagram: Be and C Introducing Structural Diversity. *J. Am. Chem. Soc.* **2022**, *144*, 5155–5162.
- [20] Pallikara, I.; Kayastha, P.; Skelton, J. M.; Whalley, L. D. The physical significance of imaginary phonon modes in crystals. *Electron. Struct.* **2022**, *4*, 033002.
- [21] Pavone, P.; Baroni, S.; de Gironcoli, S. $\alpha \leftrightarrow \beta$ phase transition in tin: A theoretical study based on density-functional perturbation theory. *Phys. Rev. B* **1998**, *57*, 10421–10423.
- [22] Pavone, P. Old and new aspects in lattice-dynamical theory. *Journal of Physics: Condensed Matter* **2001**, *13*, 7593–7610.
- [23] Masago, A.; Shirai, K.; Katayama-Yoshida, H. Crystal stability of α - and β -boron. *Phys. Rev. B* **2006**, *73*, 104102.
- [24] van Setten, M. J.; Uijtewaal, M. A.; de Wijs, G. A.; de Groot, R. A. Thermodynamic Stability of Boron: The Role of Defects and Zero Point Motion. *J. Am. Chem. Soc.* **2007**, *129*, 2458–2465.
- [25] Stoffel, R. P.; Wessel, C.; Lumey, M.-W.; Dronskowski, R. Ab Initio Thermochemistry of Solid-State Materials. *Angew. Chem. Int. Ed.* **2010**, *49*, 5242–5266.
- [26] Zhang, R. F.; Lin, Z. J.; Mao, H.-K.; Zhao, Y. Thermodynamic stability and unusual strength of ultra-incompressible rhenium nitrides. *Phys. Rev. B* **2011**, *83*, 060101.
- [27] Deringer, V. L.; Stoffel, R. P.; Dronskowski, R. Thermochemical Ranking and Dynamic Stability of TeO₂ Polymorphs from Ab Initio Theory. *Crystal Growth & Design* **2014**, *14*, 871–878.
- [28] Deringer, V. L.; Stoffel, R. P.; Dronskowski, R. Vibrational and thermodynamic properties of GeSe in the quasiharmonic approximation. *Phys. Rev. B* **2014**, *89*, 094303.
- [29] White, M. A.; Cerqueira, A. B.; Whitman, C. A.; Johnson, M. B.; Ogitsu, T. Determination of Phase Stability of Elemental Boron. *Angew. Chem. Int. Ed.* **2015**, *54*, 3626–3629.
- [30] Nyman, J.; Pundyke, O. S.; Day, G. M. Accurate force fields and methods for modelling organic molecular crystals at finite temperatures. *Phys. Chem. Chem. Phys.* **2016**, *18*, 15828–15837.
- [31] Skelton, J. M.; Burton, L. A.; Oba, F.; Walsh, A. Chemical and Lattice Stability of the Tin Sulfides. *J. Phys. Chem. C* **2017**, *121*, 6446–6454.
- [32] Pallikara, I.; Skelton, J. M. Phase stability of the tin monochalcogenides SnS and SnSe: a quasi-harmonic lattice-dynamics study. *Phys. Chem. Chem. Phys.* **2021**, *23*, 19219–19236.
- [33] Bartel, C. J. Review of computational approaches to predict the thermodynamic stability of inorganic solids. *Journal of Materials Science* **2022**, *57*, 10475–10498.
- [34] Kresse, G.; Furthmüller, J. Efficient iterative schemes for *ab initio* total-energy calculations using a plane-wave basis set. *Phys. Rev. B* **1996**, *54*, 11169–11186.
- [35] Kresse, G.; Furthmüller, J. Efficiency of ab-initio total energy calculations for metals and semiconductors using a plane-wave basis set. *Computational Materials Science* **1996**, *6*, 15 – 50.
- [36] Blöchl, P. E. Projector augmented-wave method. *Phys. Rev. B* **1994**, *50*, 17953–17979.
- [37] Kresse, G.; Joubert, D. From ultrasoft pseudopotentials to the projector augmented-wave method. *Phys. Rev. B* **1999**, *59*, 1758–1775.
- [38] Perdew, J. P.; Ruzsinszky, A.; Csonka, G. I.; Vydrov, O. A.; Scuseria, G. E.; Constantin, L. A.; Zhou, X.; Burke, K. Restoring the Density-Gradient Expansion for Exchange in Solids and Surfaces. *Phys. Rev. Lett.* **2008**, *100*, 136406.
- [39] Momma, K.; Izumi, F. VESTA 3 for three-dimensional visualization of crystal, volumetric and morphology data. *Journal of Applied Crystallography* **2011**, *44*, 1272–1276.
- [40] Becke, A. D.; Edgecombe, K. E. A simple measure of electron localization in atomic and molecular systems. *The Journal of Chemical Physics* **1990**, *92*, 5397–5403.
- [41] Savin, A.; Jepsen, O.; Flad, J.; Andersen, O. K.; Preuss, H.; von Schnering, H. G. Electron Localization in Solid-State Structures of the Elements: the Diamond Structure. *Angew. Chem. Int. Ed. Engl.* **1992**, *31*, 187–188.
- [42] Gatti, C. Chemical bonding in crystals: new directions. *Zeitschrift für Kristallographie* **2005**, *220*, 399–457.
- [43] Chen, K.; Kamran, S. Bonding Characteristics of TiC and TiN. Modeling and Numerical Simulation of Material Science **2013**, *3*, 7–11.
- [44] Le Page, Y.; Saxe, P. Symmetry-general least-squares extraction of elastic data for strained materials from *ab initio* calculations of stress. *Phys. Rev. B* **2002**, *65*, 104104.
- [45] Wu, X.; Vanderbilt, D.; Hamann, D. R. Systematic treatment of displacements, strains, and electric fields in density-functional perturbation theory. *Phys. Rev. B* **2005**, *72*, 035105.
- [46] Blonsky, M. N.; Zhuang, H. L.; Singh, A. K.; Henig, R. G. Ab Initio Prediction of Piezoelectricity in Two-Dimensional Materials. *ACS Nano* **2015**, *9*, 9885–9891.
- [47] Pashartis, C.; van Setten, M.; Houssa, M.; Pourtois, G. On the elastic tensors of ultra-thin films: A study of ruthenium. *Applied Surface Science* **2022**, *592*, 153194.
- [48] Born, M.; Huang, K. *Dynamical theory of crystal lattices*; Clarendon Press: Oxford, 1954.
- [49] Wu, Z.-j.; Zhao, E.-j.; Xiang, H.-p.; Hao, X.-f.; Liu, X.-j.; Meng, J. Crystal structures and elastic properties of superhard IrN₂ and IrN₃ from first principles. *Phys. Rev. B* **2007**, *76*, 054115.
- [50] Andrew, R. C.; Mapasha, R. E.; Ukpong, A. M.; Chetty, N. Mechanical properties of graphene and boronitrene. *Phys. Rev. B* **2012**, *85*, 125428.
- [51] Baroni, S.; de Gironcoli, S.; Dal Corso, A.; Giannozzi, P. Phonons and related crystal properties from density-functional perturbation theory. *Rev. Mod. Phys.* **2001**, *73*, 515–562.
- [52] Gonze, X. Perturbation expansion of variational principles at arbitrary order. *Phys. Rev. A* **1995**, *52*, 1086–1095.
- [53] Gonze, X. Adiabatic density-functional perturbation theory. *Phys. Rev. A* **1995**, *52*, 1096–1114.

- [54] Peng, B.; Xu, K.; Zhang, H.; Ning, Z.; Shao, H.; Ni, G.; Li, J.; Zhu, Y.; Zhu, H.; Soukoulis, C. M. 1D SbSeI, SbSI, and SbSBr With High Stability and Novel Properties for Microelectronic, Optoelectronic, and Thermoelectric Applications. Adv. Theory Simul. **2018**, 1, 1700005.
- [55] Lange, G. F.; Bouhon, A.; Monserrat, B.; Slager, R.-J. Topological continuum charges of acoustic phonons in two dimensions and the Nambu-Goldstone theorem. Phys. Rev. B **2022**, 105, 064301.
- [56] Huang, L.-F.; Gong, P.-L.; Zeng, Z. Phonon properties, thermal expansion, and thermomechanics of silicene and germanene. Phys. Rev. B **2015**, 91, 205433.
- [57] Huang, L.-F.; Lu, X.-Z.; Tennesen, E.; M.Rondinelli, J. An efficient ab-initio quasiharmonic approach for the thermodynamics of solids. Computational Materials Science **2016**, 120, 84–93.
- [58] Peng, B.; Bravić, I.; MacManus-Driscoll, J. L.; Monserrat, B. Topological semimetallic phase in PbO_2 promoted by temperature. Phys. Rev. B **2019**, 100, 161101.
- [59] Feng, J.; Xiao, B.; Zhou, R.; Pan, W.; Clarke, D. R. Anisotropic elastic and thermal properties of the double perovskite slab-rock salt layer $\text{Ln}_2\text{SrAl}_2\text{O}_7$ (Ln=La, Nd, Sm, Eu, Gd or Dy) natural superlattice structure. Acta Materialia **2012**, 60, 3380–3392.
- [60] Dove, M. T. Introduction to Lattice Dynamics; Cambridge University Press, 1993.
- [61] Togo, A.; Oba, F.; Tanaka, I. First-principles calculations of the ferroelastic transition between rutile-type and CaCl_2 -type SiO_2 at high pressures. Phys. Rev. B **2008**, 78, 134106.
- [62] Togo, A.; Tanaka, I. First principles phonon calculations in materials science. Scripta Materialia **2015**, 108, 1–5.